Science Advances

AAAS

advances.sciencemag.org/cgi/content/full/2/8/e1600881/DC1

Supplementary Materials for

Kinetic control of the coverage of oil droplets by DNA-functionalized colloids

Darshana Joshi, Dylan Bargteil, Alessio Caciagli, Jerome Burelbach, Zhongyang Xing, André S. Nunes, Diogo E. P. Pinto, Nuno A. M. Araújo, Jasna Brujic, Erika Eiser

Published 5 August 2016, *Sci. Adv.* **2**, e1600881 (2016)
DOI: 10.1126/sciadv.1600881

The PDF file includes:

Other Supplementary Material for this manuscript includes the following:
(available at advances.sciencemag.org/cgi/content/full/2/8/e1600881/DC1)

- video S1 (.avi format). Dynamics of DNA-anchored colloids in gas phase imaged with 30 frames/s, focusing on the south pole.
- video S2 (.avi format). Dynamics of colloids aggregated into 2D crystals on OD surfaces imaged with 5 frames/s, focusing on the south pole.
- video S3 (.avi format). Single 1-μm large colloids DNA-anchored to the OD imaged with 50 frames/s.
- video S4 (.avi format). Single 1-μm large colloid diffusing freely in solution (kept in focus with a feedback mechanism), imaged with 50 frames/s.

Supplementary Materials

Supplementary Materials and Methods

Experiments.

Preparation of oil droplets (ODs). The ODs were prepared in a microfluidic device. Prior to its use the device was plasma cleaned and immediately afterwards filled with water to slow down the loss of hydrophilicity of the device walls, and tested for leaks. The channels used were 20 µm wide and 25 µm high. Firstly, 5 to 10 mM SDS solution was flushed in at 250 µL/hr in order to flood the channel. Once SDS has filled the channel, 50 cSt silicone oil (0.971 g/mL) was introduced at 25 µL/hr into the channels. Droplets formed at the junction and were collected at the outlet (Fig. 1A). We used Nemesys and Harvard pumps. ODs were stored in the fridge in a 10 mM SDS solution – they remained stable for a minimum of one year. The SDS was purchased from Sigma and used as received. All solutions were prepared in deionized water.

PLL-PEG-Biotin adsorption on the oil droplet surface. In fig. S1 we show the calibration curve for the adsorption of PLL- PEG-bio on the SDS stabilized ODs. We measured the fluorescence attached on the ODs upon adding a fixed amount of fluorescently labeled streptavidin to each sample.

Melt temperature between hard PS spheres grafted with complementary ssDNA. We determined the melt temperature T_m between 0.52 µm large PS colloids in bulk solution (4 mM Tris pH 7-8, 50 mM NaCl); no surfactants were added but we did use density matching with sucrose, preventing the colloids from sedimenting. For clarity we used a colloid volume fraction, $\Phi_c \sim$ 5%. The samples were heated to 50ºC and then slowly cooled to room temperature and subsequently heated again using a custom-build Peltier heating/cooling-stage. In fig. S2 a sequence of fluorescence images is shown for a typical cooling cycle. We identify the melt temperature to be between 35 and 34ºC—it is the temperature at which the DNA-attraction is switched on, which is equivalent to the temperature at which spinodal decomposition into a colloid rich and colloid poor sample sets in (*38*). Upon heating, the colloidal gel melts in the very same narrow temperature window.

Geometry of the PLL-PEG-biotin chain at the oil-water interface. Figure S3 is a schematic of how the PLL-PEG-bio chains arrange on the oil-droplet surface stabilized by the negatively charged surfactants SDS (sodium dodecyl sulphate). The effective head-group size of the surfactant is roughly 50 $Å^2$ corresponding to a radius of about 0.3 nm (*42*). The PLL-PEG-bio chains have 137 repeat units, with PEG chains of molecular weight of 2 kDa or PEG-bio chains with 3.5 kDa anchored to every 3.5 repeat lysine unite on average. This corresponds to an inter-anchor spacing of about 1.25 nm. The radius of gyration of a free 2 kDa PEG chain in good solvent condition is about 1.8 nm (*31*). Note that the longer 3.5 kDa chains carrying the biotin ends will have an even larger R_g. This means the PEG chains must be in a brush configuration when the PLL is lying flat on the OD surface. Moreover, the osmotic pressure building up between the PEG chains will force the PLL chain to be in a stretched configuration on the OD surface.

Microrheology. Using the *x*- and *y*-displacements obtained from particle tracking measurements we extracted the viscoelastic properties the 1.2 μm large colloids experience when hybridized to the oil-water interface. We use the fact that the Laplace transform of the diffusion coefficient can be expressed as the Laplace transform of the velocity auto-correlation function

$$D(s) = \frac{k_B T}{6\pi G(s) R s} = \frac{\mathcal{L}(\langle v_x(0) v_x(t) \rangle)}{s}$$

Here, $G(s)$ is the Laplace transform of the complex shear modulus (*20*). The Laplace transform of the time-dependent velocity correlation function, $C(s) = \mathcal{L}(\langle v_x(0) v_x(t) \rangle)$, was obtained with a loss-free coarse-graining algorithm, which was fed with the position-data. Evans et al. and Yanagishima et al. (*20*) showed that $C(s) = \mathcal{L}(C(t))$ can be expressed by

$$C(s) = \frac{\sum_i a_i \exp(-s t_i)}{s^2} + \frac{c(t=0)}{s}$$

The first term describes the contribution from the decaying velocity-correlation function, which corresponds to a series of delta functions with amplitude a_i. The second term comes from the fact that the first term of $C(t)$ at time $t = 0$ adds a finite value. The elastic and the viscous moduli G' and G'' were extracted from $C(s) = \mathcal{L}(C(t))$ by replacing s by $i\omega$ and using the fact that $G^*(\omega) = G'(\omega) + iG''(\omega)$. The average loss modulus G'' extracted from the tracks of 1.2 μm particles hybridized to the liquid-liquid interface is shown in fig. S4.

Simulations.

Stochastic model. To understand the enhancement of the binding density on the bulk concentration of colloids we studied a stochastic model schematically summarized in fig. S5.

For simplicity, the interface is described as a two-dimensional discrete (square) lattice of linear length L, in units of lattice sites. The interface is initially covered with a density ρ_p of squared patches (blue squares in the figure), of linear length $l_p = 1$, in units of lattice sites. The patches, are irreversibly bound to the interface and diffuse around with a diffusion coefficient D_p (fig. S5(a)), solely interacting through excluded volume.

Squared colloids of linear length $l_C = 2$ (green in fig. S5) arrive to the interface at a flux F (number of colloids per unit area and time), which is a monotonic increasing function of the bulk concentration. Colloids irreversibly bind to a patch, forming a colloid-patch complex, if they overlap it (fig. S5(a) and (c)) and don't overlap a previously bound colloid (fig. S5(d)). Since we are interested in the initial stage of binding and the diffusion of colloid-patch complexes is much lower than D_p, we assume that a complex does not diffuse. Nevertheless, a free patch can still diffuse and bind to the colloid, if it goes underneath the colloid-patch complex without

overlapping the already present patch, thus forming a raft. We performed kinetic Monte Carlo simulations for two different values of the patch density (ρ_p = {0.01, 0.1}). We define the binding density as the number of colloids per lattice unit. Figure S6 shows the binding density as a function of the flux of colloids. The binding density is rescaled by the patch density, such that unity corresponds to one colloid per patch and the flux is rescaled by D_p. The binding density monotonically increases with F/D_p as suggested by the experimental results. This is likely a result of the competition between two different time scales: the inter-arrival time and the Brownian time. The former is the typical time between two consecutive attempts of colloidal binding per lattice site and it corresponds to the inverse of the flux. The latter is the average time necessary for a patch to diffuse in a region corresponding to its area and it is the inverse of the diffusion time. As colloids bind to patches, the higher the ratio F/D_p the lower the probability that a patch diffuses underneath a colloid-patch complex and bind to it before a new colloid directly binds to it. Every time a patch binds to an already formed colloid-patch complex, the number of available patches is reduced. Thus, the binding density increases with F/D_p. Note that the effect is even more pronounced for higher patch densities (black and red curves in fig. S6), as the typical distance between patches (or between patches and colloid-patch complexes) is shorter favoring the binding of free patches to previously formed complexes.

Aggregation mediated by depletion. To study the aggregation of colloid-patch complexes mediated by the depletion of SDS micelles, we performed Brownian dynamics simulations on a curved interface where the interaction between colloid-patch complexes is considered pairwise and described by the super- position of a Yukawa (repulsive) potential

$$U_Y = B_Y \frac{\exp(-(r - r_0)/r_0)}{r - r_0}$$

where B_Y is a constant with units of energy, and the Asakura-Oosawa (AO) entropic potential for depletion

$$U_{AO} = V_{AO}[1 - 3/4((r - r_0)/r_0 + 1/16((r - r_0)/r_0)^3]$$

where r is the distance between colloids, r_0 is the diameter of a colloid, and V_{AO} the strength of interaction. Note that V_{AO} scales linearly with the concentration of depletant (SDS micelles). In the main text we show snapshots for different strengths of the AO potential (see fig. S7). Figure 2(D) corresponds to V_{AO} = 0, i.e., the case below the critical concentration of SDS where the concentration of SDS micelles in the bulk is negligible. As we increase V_{AO} we observe a transition from a gas-like structure to crystalline-like order.

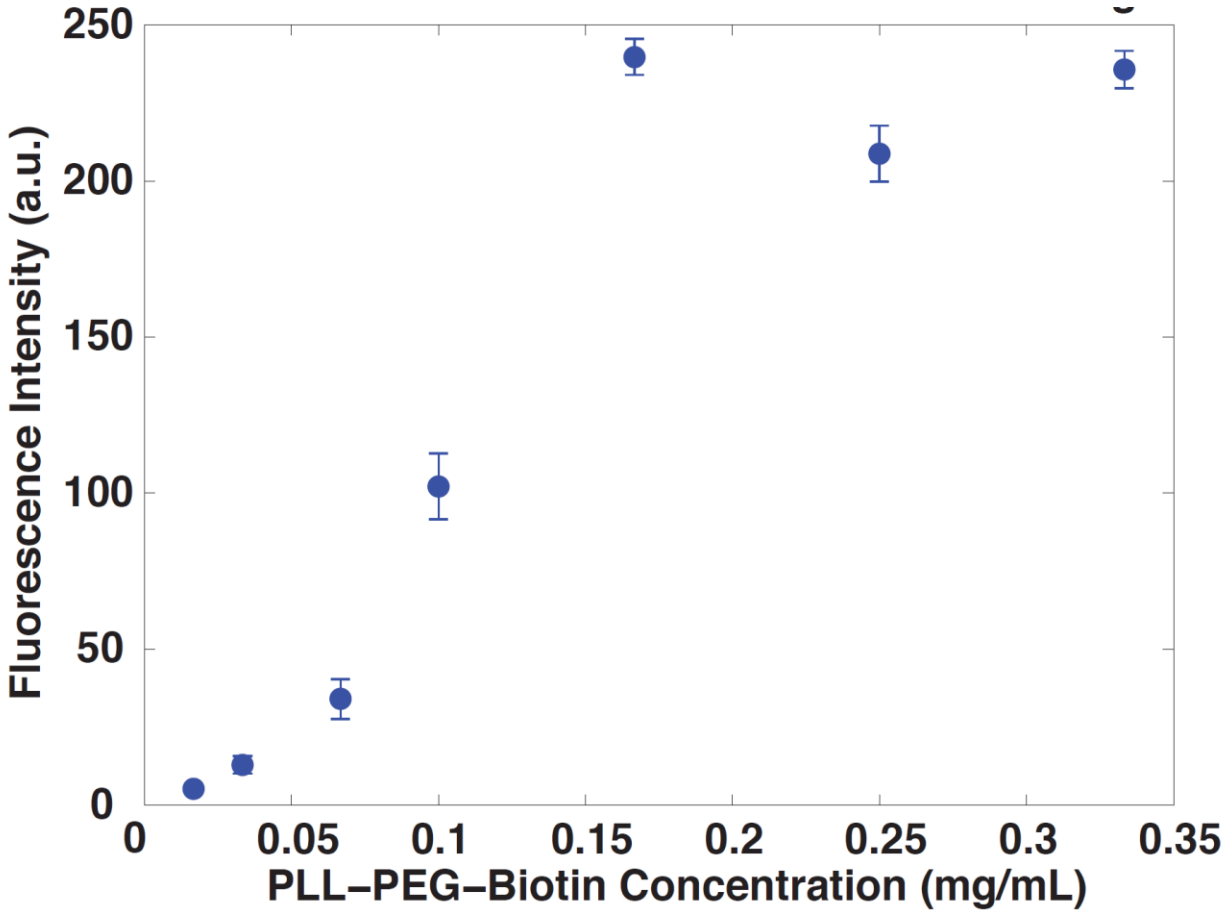

fig. S1. Calibration curve for the surface coverage of PLL-PEG-bio. Fluorescence intensities of the Texas Red labelled streptavidin were used as a measure for the approximate surface coverage of PLL-PEG-Biotin on the ODs obtained by titrating a fixed volume of ODs (25 µL) in suspending solution (2 mM SDS, 50 mM NaCl) with a solution of PLL-PEG-bio in an overall volume of 300 µL.

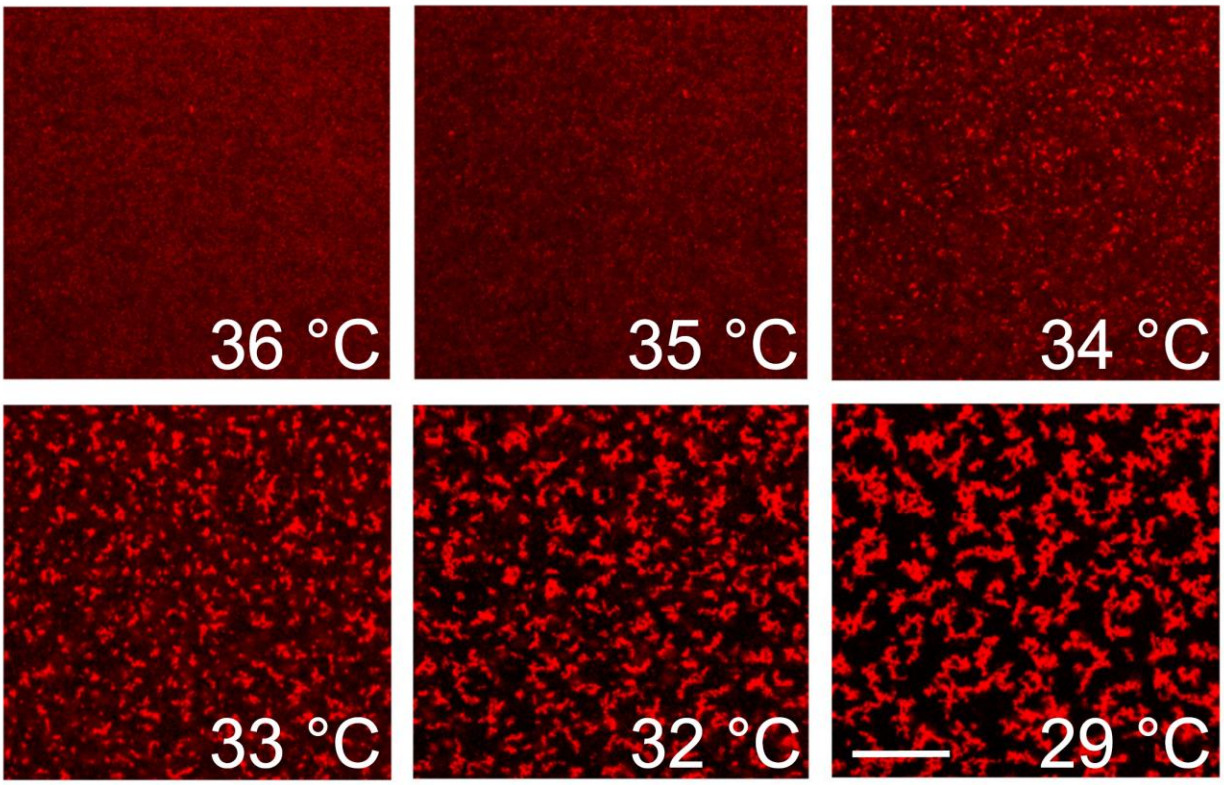

fig. S2. **Phase transition of the DNA-functionalized PS spheres.** Fluorescence-microscopy images showing the transition from a high temperature uniform gaseous phase to a low temperature gelled phase (upon cooling) in a single component system of red fluorescent 0.52 μm large colloids, where half of the colloids were coated with ssDNA, **A**, and the other half with **A′ DNA**, in 4 mM Tris pH 7-8, 50 mM NaCl solution. The scale bar is ∼50 μm.

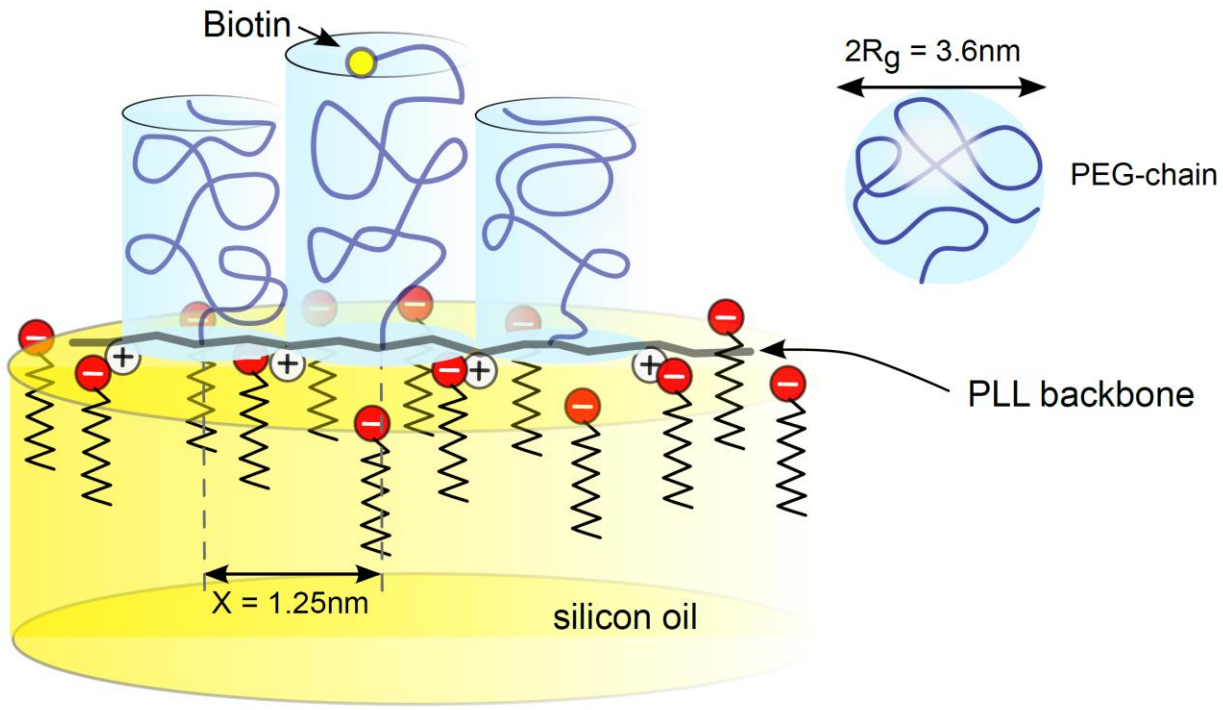

fig. S3. **Schematics of the oil-water interface.** PLL-PEG-biotin chain adsorbed to the oil-water interface through the Coulomb attraction between the positive charges on the polylysine backbone and the negatively charged head groups of the SDS surfactants. Every 3.5 lysine repeat units a PEG chain is attached, half of them with molecular weight of 2 kD and the other, holding a biotin end, with 3.5 kD. The lysine monomer is 0.355 nm long. The radius of gyration, *Rg* , of the unbound PEG(2 kD) chain is $\sim$1.8 nm.

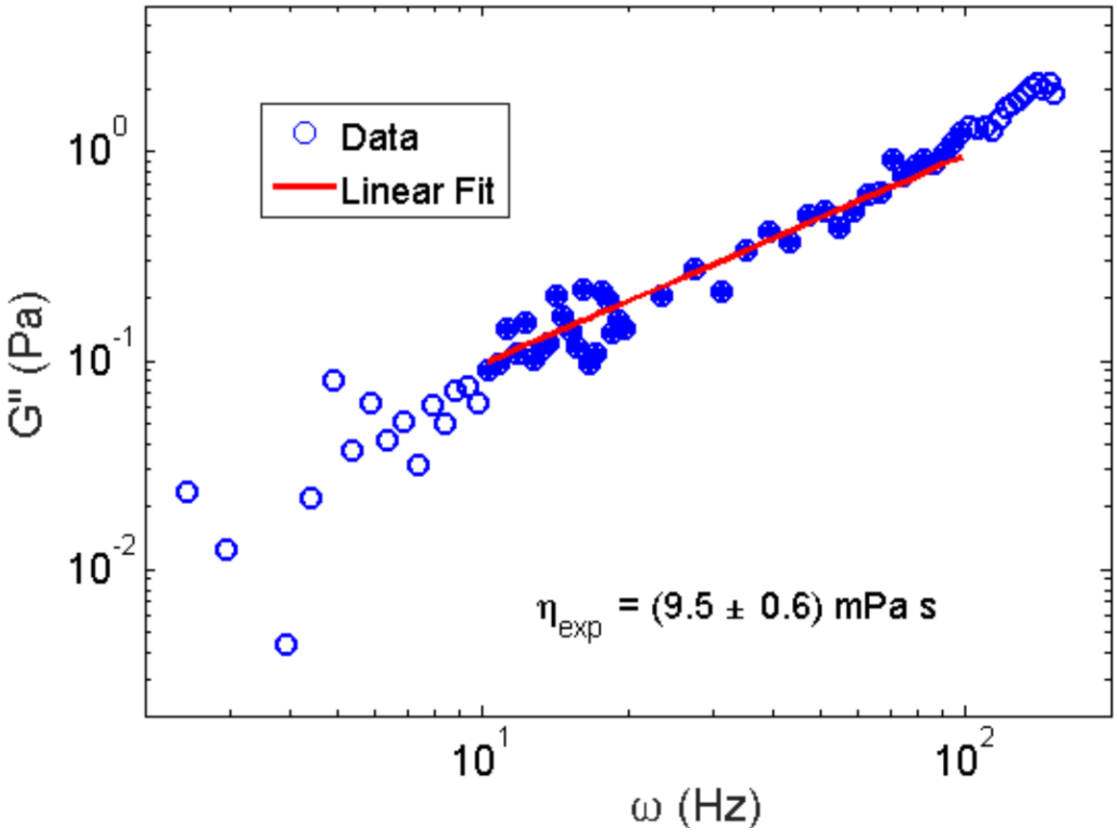

fig. S4. **Microrheology on the oil-water interface.** Loss modulus *G''* as function of frequency for 1.2 µm particles bound to the oil-water interface: the data were averaged over 5 independent particle tracks. The open circles show the full data set, while the solid circles represent a subset of these data points we fitted linearly to extract the viscosity ηexp, which follows the expected scaling $G'' \propto \eta\omega$.

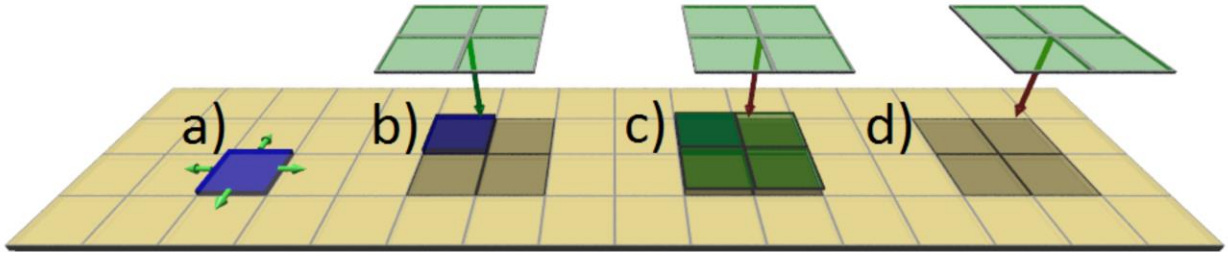

fig. S5. Schematic representation of the stochastic model. The interface is described as a square lattice with an initial density of patches (blue). Patches diffuse (**a**) and interact through excluded volume. Square colloids (green) arrive at the interface with a constant flux and irreversibly bind to an unbound patch if it overlaps with it (**b**). The binding fails if the new colloid either overlaps a previously bounded colloid (**c**) or lands in a region without patches (**d**).

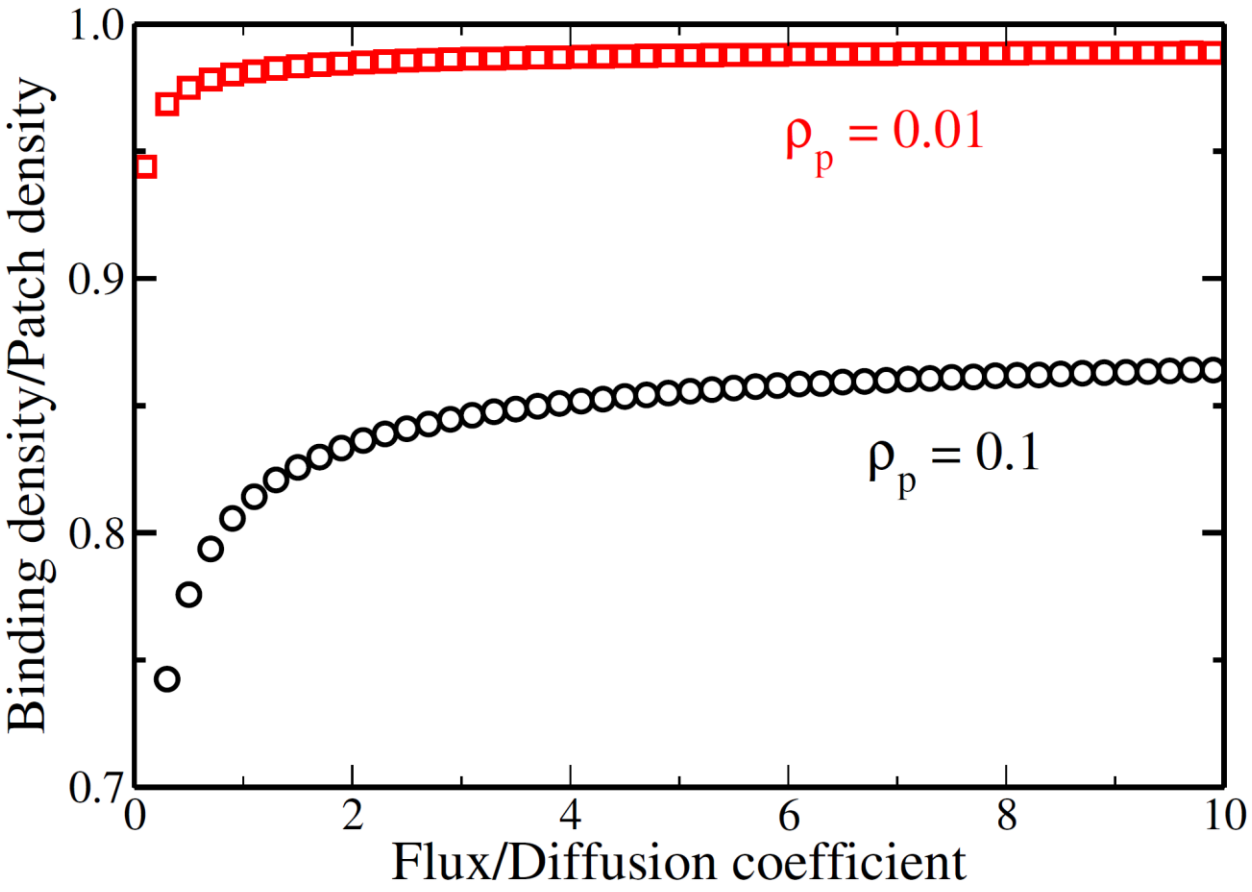

fig. S6. Dependence of the binding density on the flux and diffusion coefficient. Binding density, defined as the number of bounded colloids per lattice site, as a function of the ratio between flux (F) of colloids and patch diffusion coefficient (D_p). The vertical axis is rescaled by the patch density (ρ_p) such that unity corresponds to one colloid per patch. The black circles are for a patch density of 0.1 and the red squares for patch density of 0.01. Results are averages over 10^3 samples on a square lattice of length $L = 10^3$, i.e., 10^6 sites.

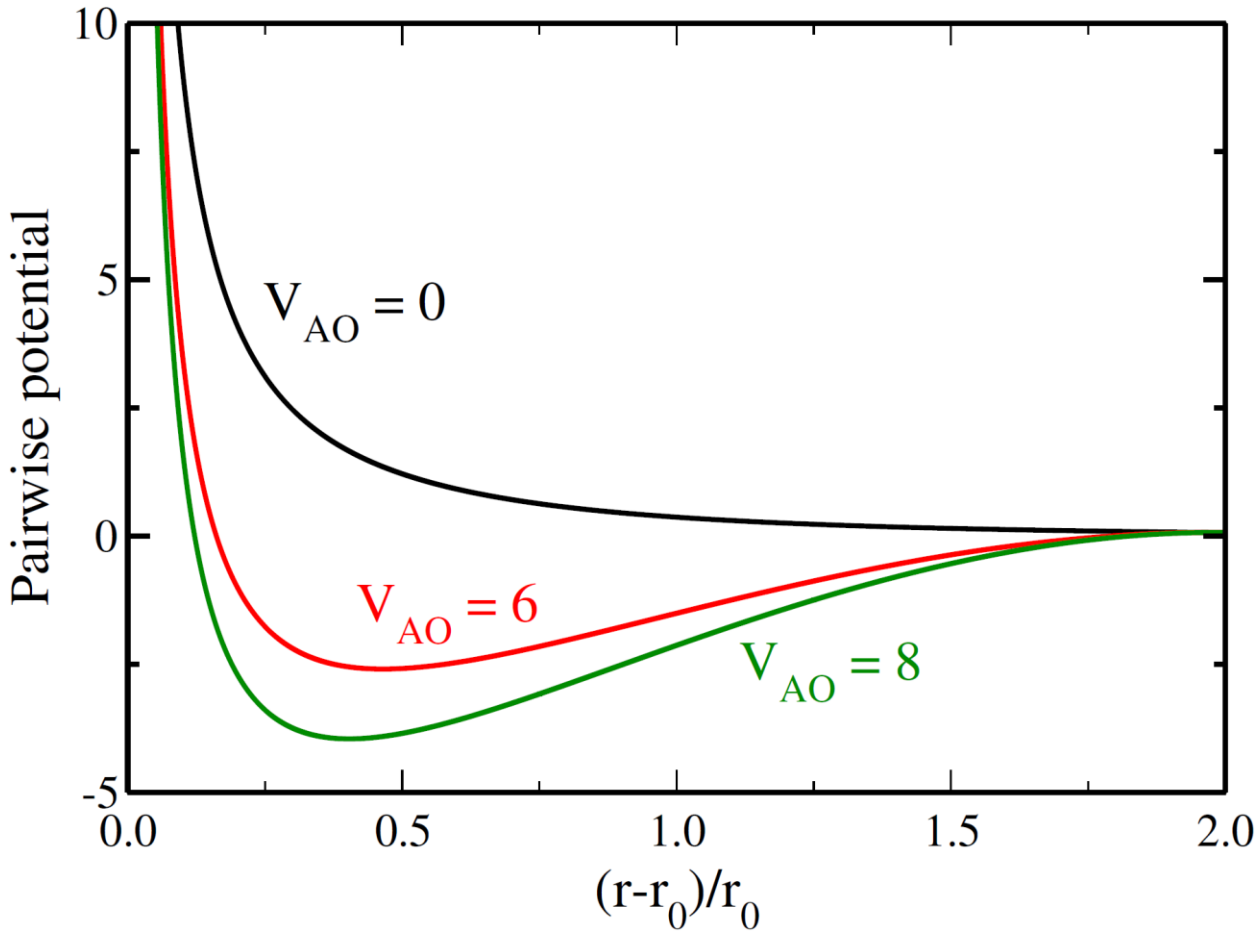

fig. S7. Pairwise potential for different strengths AO potential. The colloid-colloid pairwise interaction is described by a superposition of a repulsive Yukawa and an attractive Asakura-Oosawa potential. For $V_{AO} = 0$ the total potential is purely repulsive, while for $V_{AO} = \{6, 8\}$, it yields a minimum.

table S1. Various DNA constructs used in the experiments. A typical DNA construct carries a biotin functionalisation on the 5' end, a double stranded (ds)DNA spacer (assembled by hybridizing X/X' pair), flexible joints (TTTTT) and a 'sticky overhang' at the 3' end (marked in red).

Name	DNA Construct
B	5' – Biotin – TTTTT – X – TTTTT – CG CAG CAC C – 3'
A	5' – Biotin – TTTTT – X – TTTTT – CCG GCC – 3'
A'	5' – Biotin – TTTTT – X – TTTTT – GGC CGG – 3'
X	5'- GAG GAG GAA AGA GAG AAA GAA GGA GAG GAG AAG GGA GAA AAG AGA GAG GGA AAG AGG GAA -3'
X'	5'- TTC CCT CTT TCC CTC TCT CTT TTC TCC CTT CTC CTC TCC TTC TTT CTC TCT TTC CTC CTC -3'